



Optimization of artificial neural networks for prediction of the unit cell parameters in orthorhombic perovskites. Comparison with multiple linear regression

Igor Kuzmanovski*, Slobotka Aleksovska

Institut za hemija, PMF, Univerzitet "Sv. Kiril i Metodij", PO Box 162, 1001 Skopje, Macedonia

Received 5 January 2003; accepted 4 May 2003

Abstract

The unit cell parameters (a , b , c) of orthorhombic perovskites (of $A^{2+}B^{4+}O_3$ and $A^{3+}B^{3+}O_3$ type) were predicted both using multiple linear regression analysis (MLR) and two types of artificial neural networks (ANN). In these analyses, 70 compounds of above perovskite type were included: 47 in calibration set and 23 in test set, which were randomly chosen. In multiple linear regression, the unit cell parameters of 47 perovskites were expressed as bilinear function of the effective ionic radii of A and B cations, and then, using the obtained regression equation, the unit cell parameters of 23 perovskites were calculated and compared with the experimental data. Predictions using the same sets and the same dependent and independent variables were also done by feed-forward and cascade-forward ANN. The two different ANN models were compared to MLR model by F -test using their root mean square error ($RMSEP$). Although the two models give excellent results, it could be concluded that ANN have significantly better prediction abilities compared to MLR.

© 2003 Elsevier B.V. All rights reserved.

Keywords: Perovskites; Linear regression; Cell parameter

1. Introduction

1.1. Perovskites

The perovskites are wide group of isotypic inorganic compounds with general formula ABO_3 [1]. They are one of the most interesting groups of inorganic compounds both from fundamental sci-

entific and applicative point of view. This is due not only to its wide occurrence, but also to a series of interesting and useful physicochemical properties. Therefore, perovskite-type materials are of particular technical importance. For example, it is well known that some perovskites exhibit ferromagnetic, ferroelectric, pyroelectric and piezoelectric properties. It should be pointed out that number of perovskites exhibit superconductivity. Actually, the most interesting fact is that all the known high temperature superconductors have modified or defect perovskite structures. Also, perovskites are suitable compounds for semiconducting thin film materials. Recently, perovskites have been investigated for use as electro-

* Corresponding author. Tel.: +398-2-3117-055; fax: +398-2-3226-865.

E-mail address: shigor@iunona.pmf.ukim.edu.mk
(I. Kuzmanovski).

des in fuel cells. They can be used in the industry as catalysts, as well [1,2].

Firstly, it was thought that perovskites have an ideal cubic structure, but later was found that they could be divided in several isostructural and isomorphous subgroups with orthorhombic, tetragonal, rhombohedral, etc. structures. In each group, compounds ions in different oxidation states (for example: $A^{2+}B^{4+}O_3$, $A^{3+}B^{3+}O_3$, $A^{1+}B^{5+}O_3$) can exist and, also, mixed cation structures such as: $A(B'_x B''_{1-x})O_3$, $A(B'_{1-x} B''_x)O_3$, $A'_x A''_{1-x} BO_3$, etc.

Taking into consideration the technical use of perovskite type materials, the prediction of their structures and properties is very important. Since we have already used multiple linear regression for predicting the unit cell parameters, as well as for prediction of the complete crystal structure [3–6], we continue with similar work in the field of perovskites. In this work, the unit cell parameters in isomorphous group of perovskites are predicted as a function of effective ionic radii of the cations in perovskite structure using multiple linear regression and artificial neural networks. For this purpose, the orthorhombic perovskites ($A^{2+}B^{4+}O_3$ and $A^{3+}B^{3+}O_3$) which crystallize in $GdFeO_3$ structural type, space group P_{bnm} with $Z=4$, were chosen. The mixed cation structures such as: $A(B'_x B''_{1-x})O_3$, etc. were not taken into consideration in this work. Although some preliminary investigations using average ionic radii for the cations in B-position in mixed cation structure have given good results, only the results for the orthorhombic ABO_3 perovskites will be discussed.

1.2. Artificial neural networks

In the last decade, the ANN, computation systems (implemented the most often in terms of software) designed on the basis of the biological neurons capable for parallel signal processing, have been proven as valuable and efficient method for handling of noisy, nonlinear and incomplete multivariate data [7] in different aspects of chemistry [9] and today are valuable tool for chemometricians. ANN and their application in chemistry in details are described in literature [8,9].

In this work, three-layered feed-forward (Fig. 1a) and cascade-forward (Fig. 1b) ANNs were used with one input, one output and one hidden layer. Compared

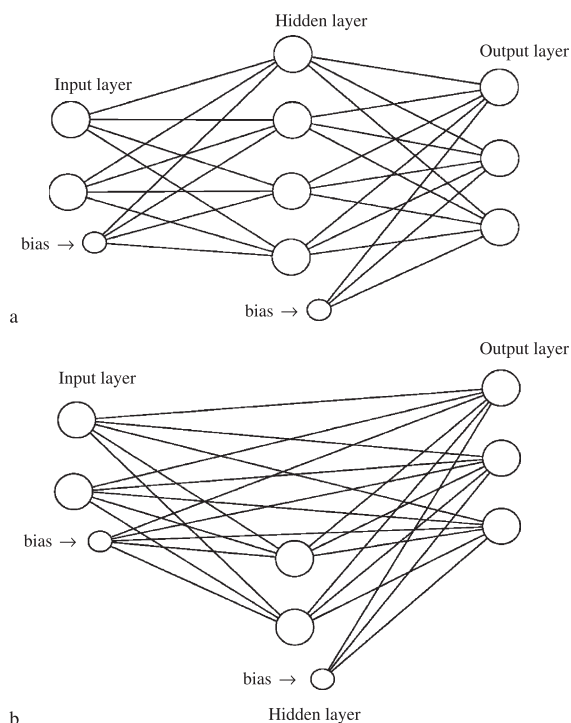


Fig. 1. Feed-forward (a) and cascade-forward (b) artificial neural networks.

to feed-forward neural networks which are designed for nonlinear modeling of the data, and are most often used, direct connection between input and output neurons (with linear transfer function) in cascade-forward neural networks are capable of modeling only linear part in the relation of input and output data, while the neurons in the hidden layer (with nonlinear—sigmoid transfer function) models only the nonlinear part of the relationship between input and output data. Usually, the cascade-forward networks are capable of solving the same problem with smaller number of neurons in the hidden layer compared to feed-forward networks, but since the number of weights in cascade-forward ANNs is bigger their optimization is slower compared to feed-forward networks.

2. Data analysis

The values for the effective ionic radii of A and B cation (independent variables) were taken from Shan-

Table 1

Input data (effective ionic radii and the unit cell parameters) used for optimization in both models

	Formula	$r(A)/\text{\AA}$	$r(B)/\text{\AA}$	$a/\text{\AA}$	$b/\text{\AA}$	$c/\text{\AA}$	Ref.
<i>Calibration set</i>							
1	BiRhO ₃	1.03	0.665	5.354	5.813	7.776	[11]
2	DyAlO ₃	0.912	0.535	5.21	5.31	7.4	[1]
3	DyFeO ₃	0.912	0.645	5.3	5.6	7.62	[1]
4	ErFeO ₃	0.89	0.645	5.263	5.582	7.591	[12]
5	ErVO ₃	0.89	0.64	5.254	5.589	7.554	[13]
6	EuFeO ₃	0.947	0.645	5.371	5.611	7.686	[1]
7	EuScO ₃	0.947	0.745	5.502	5.752	7.954	[14]
8	GdAlO ₃	0.938	0.535	5.247	5.304	7.447	[1]
9	GdCrO ₃	0.938	0.615	5.312	5.514	7.611	[15]
10	GdScO ₃	0.938	0.745	5.4908	5.7559	7.9382	[16]
11	GdVO ₃	0.938	0.64	5.35	5.62	7.643	[13]
12	HoVO ₃	0.901	0.64	5.278	5.601	7.573	[17]
13	LaCrO ₃	1.032	0.615	5.477	5.514	7.755	[1]
14	LaGaO ₃	1.032	0.62	5.496	5.524	7.787	[15]
15	LaInO ₃	1.032	0.8	5.723	5.914	8.207	[1]
16	LuFeO ₃	0.861	0.645	5.213	5.547	7.565	[12]
17	LuVO ₃	0.861	0.64	5.216	5.571	7.529	[17]
18	NdFeO ₃	0.983	0.645	5.453	5.584	7.786	[12]
19	NdGaO ₃	0.983	0.62	5.426	5.502	7.706	[15]
20	NdScO ₃	0.983	0.745	5.5772	5.7754	8.0037	[16]
21	NdVO ₃	0.983	0.64	5.451	5.582	7.738	[17]
22	PrFeO ₃	0.99	0.645	5.482	5.578	7.786	[12]
23	PrGaO ₃	0.99	0.62	5.465	5.495	7.729	[15]
24	PrVO ₃	0.99	0.64	5.474	5.572	7.76	[17]
25	PuCrO ₃	1	0.615	5.46	5.51	7.76	[1]
26	ScAlO ₃	0.745	0.535	4.9355	5.2313	7.2007	[18]
27	SmAlO ₃	0.958	0.535	5.295	5.301	7.503	[19]
28	SmFeO ₃	0.958	0.645	5.4	5.597	7.711	[12]
29	SmInO ₃	0.958	0.8	5.589	5.886	8.082	[1]
30	TbFeO ₃	0.923	0.645	5.326	5.602	7.635	[12]
31	TbVO ₃	0.923	0.64	5.319	5.621	7.605	[17]
32	TmVO ₃	0.88	0.64	5.244	5.582	7.548	[17]
33	YAlO ₃	0.9	0.535	5.18	5.33	7.375	[20]
34	YFeO ₃	0.9	0.645	5.279	5.587	7.599	[21]
35	YTiO ₃	0.9	0.67	5.327	5.618	7.591	[22]
36	YbFeO ₃	0.868	0.645	5.233	5.547	7.565	[12]
37	YbVO ₃	0.868	0.64	5.23	5.578	7.54	[17]
38	BaPrO ₃	1.35	0.85	6.2137	6.1787	8.7261	[23]
39	BaPuO ₃	1.35	0.86	6.219	6.193	8.744	[24]
40	CaTiO ₃	1	0.605	5.3796	5.4423	7.6401	[25]
41	CaVO ₃	1	0.58	5.326	5.352	7.547	[1]
42	CaZrO ₃	1	0.72	5.59	5.76	8.02	[26]
43	CdTiO ₃	0.95	0.605	5.3053	5.4423	7.6401	[27]
44	SrHfO ₃	1.18	0.71	5.769	5.78	8.14	[28]
45	SrRuO ₃	1.18	0.62	5.5304	5.567	7.8446	[29]
46	SrUO ₃	1.18	0.89	6.01	6.17	8.6	[1]
47	SrZrO ₃	1.18	0.72	5.79	5.805	8.172	[30]
<i>Test set</i>							
1	CeVO ₃	1.01	0.64	5.514	5.557	7.808	[31]
2	DyVO ₃	0.912	0.64	5.292	5.598	7.586	[13]

Table 1 (continued)

	Formula	$r(A)/\text{\AA}$	$r(B)/\text{\AA}$	$a/\text{\AA}$	$b/\text{\AA}$	$c/\text{\AA}$	Ref.
3	EuAlO ₃	0.947	0.535	5.271	5.292	7.458	[1]
4	EuVO ₃	0.947	0.64	5.364	5.617	7.645	[17]
5	GdFeO ₃	0.938	0.645	5.349	5.611	7.669	[12]
6	HoFeO ₃	0.901	0.645	5.278	5.591	7.591	[12]
7	LaFeO ₃	1.032	0.645	5.554	5.566	7.853	[32]
8	LaScO ₃	1.032	0.745	5.6748	5.7911	8.0923	[16]
9	NdCrO ₃	0.983	0.615	5.382	5.481	7.685	[33]
10	NdInO ₃	0.983	0.8	5.627	5.891	8.121	[1]
11	PrCrO ₃	0.99	0.615	5.444	5.484	7.71	[15]
12	PrScO ₃	0.99	0.745	5.615	5.776	8.029	[15]
13	PuVO ₃	1	0.64	5.48	5.61	7.78	[1]
14	SmCrO ₃	0.958	0.615	5.372	5.502	7.65	[15]
15	SmVO ₃	0.958	0.64	5.395	5.601	7.683	[17]
16	TmFeO ₃	0.88	0.645	5.251	5.576	7.584	[12]
17	YCrO ₃	0.9	0.615	5.247	5.518	7.54	[34]
18	YVO ₃	0.9	0.64	5.271	5.574	7.556	[22]
19	BaCeO ₃	1.35	0.87	6.213	6.235	8.781	[35]
20	CaSnO ₃	1	0.69	5.532	5.681	7.906	[36]
21	CaUO ₃	1	0.89	5.78	5.97	8.29	[1]
22	SrCeO ₃	1.18	0.87	6.094	6.132	8.638	[37]
23	SrPbO ₃	1.18	0.775	5.86	5.964	8.32	[38]

non [10]. The values refer to coordination number six for both cations and for high spin state for d -ions. The data for the unit cell parameters (dependent variables) for 70 different perovskites were collected from the literatures [1,11–38]. The data set was divided randomly into calibration and test set. Both, dependent and independent, variables are given in Table 1. The order of the perovskites in Table 1 was made alphabetically by the symbol of the cation in A position. It should be mentioned that $A^{3+}B^{3+}O_3$ perovskites are ordered first, and then $A^{2+}B^{4+}O_3$ perovskites follow.

2.1. Multiple linear regression

The multiple linear regression was performed using the program package STAGRAPHICS PLUS Ver. 3.0 [39]. Each unit cell parameter was expressed as bilinear function of the effective ionic radii of the cations:

$$d/\text{\AA} = e + f \times r(A)/\text{\AA} + g \times r(B)/\text{\AA} \quad (1)$$

where d is the unit cell parameter (a , b , c), and $r(A)$ and $r(B)$ are the effective ionic radii of A and B cations and f and g are regression coefficients and e is

intercept. The regression equations were found using the calibration set (consisted of 47 compounds). The obtained regression equations were used for estimation of unit cell parameters for the compounds in the test set.

2.2. Artificial neural networks

All the data (the input data—effective ionic radii as well as their corresponding outputs—parameters of the unit cell) were scaled in the interval between 0 and 1, and were stored in single data matrix. The processing of the data was carried on Intel Celeron 900 MHz PC with 256 Mb of RAM in Windows XP (Microsoft, USA) environment using Matlab 6.0 [40]. The neural networks were implemented using Neural Network Toolbox Ver. 4.0 [41] for Matlab.

The performances of different networks were evaluated in terms of root mean square error (*RMSEP*), defined as shown in Eq. (2):

$$RMSEP = \sqrt{\frac{\sum_k \sum_m (y_{k,m} - out_{k,m})^2}{mk}} \quad (2)$$

in Eq. (2), m is number of samples in the test, k represents number of dependent variables (unit cell parameters), $y_{k,m}$ is the value for the unit cell parameter m in the sample number k . The $out_{k,m}$ is the predicted value of the unit cell parameter m in the sample number k .

3. Results and discussions

3.1. Multiple linear regression

Firstly, the model was optimized using calibration set of 47 compounds (Table 1). The obtained regres-

sion equations and the adjusted coefficients of determination are given below:

$$a/\text{\AA} = 3.21 + 1.46r(\text{A})/\text{\AA} + 1.29r(\text{B})/\text{\AA}$$

$$\overline{R^2} = 0.970$$

$$b/\text{\AA} = 3.87 + 0.248r(\text{A})/\text{\AA} + 2.29r(\text{B})/\text{\AA}$$

$$\overline{R^2} = 0.960$$

$$c/\text{\AA} = 4.87 + 1.35r(\text{A})/\text{\AA} + 2.38r(\text{B})/\text{\AA}$$

$$\overline{R^2} = 0.984$$

Using the obtained regression equations, the unit cell parameters for 23 perovskites (test set) were calculated and compared with the literature data and the over all (*RMSEP*=0.0417), as well as the *RMSEP* for the unit cell parameters were calculated (Table 2).

3.2. Optimization of artificial neural networks model

The network architecture giving the best performances (smallest value for the *RMSEP* for the test set) was searched changing the number of neurons in the hidden layer (from 1 to 11), while the number of the input and output neurons was fixed and was determined by the input data for each substance (effective ionic radii) and their corresponding outputs (unit cell parameters). The number of neurons in hidden layer defines the complexity of the developed model. If the neurons in hidden layer are too few, the ANN will not be able to model the data accurately. If the number of neurons in hidden layer is too large the performances of the ANN will be reduced [42]. The weights and biases were initialized according to Nguyen–Widrow algorithm to enforce that the active regions of the layer's neurons were distributed roughly evenly over the input space. The optimization of the weights and biases was carried

Table 2
Root mean square error obtained using MLR and ANN

	$RMSEP_{\text{overall}}/\text{\AA}$	$RMSEP_a/\text{\AA}$	$RMSEP_b/\text{\AA}$	$RMSEP_c/\text{\AA}$
FF-ANN	0.0289	0.0331	0.0276	0.0253
CF-ANN	0.0251	0.0238	0.0231	0.0283
MLR	0.0417	0.0370	0.0496	0.0370

out according to Levenberg–Marquardt algorithm for back-propagation of error. Training was repeated 20 times for each network architecture.

In order to avoid overtraining of the ANNs, which could produce poor generalization abilities, the early stopping procedure was applied. The technique requires dividing of the data sets into three subsets: training set, validation set and test set. In aim to obtain as much as possible better spanning of the data into the input space, it is suitable the size of the training and validation set to be comparable. The training set (consisted of 24 samples from the calibration set—the samples marked with odd number at Table 1) was used for adjustment of the weights and biases during the training process. During the training, the performances of the networks are monitored with validation set (consisted of 24 samples from the calibration data set—the samples marked with even number at Table 1). At the beginning of the training, the error in training and validation set decreases until the network starts to overtrain the data in the training set. Then, the error in validation set starts to increase. In this study, if the error in the validation set increased for five consecutive iterations, the training

was stopped, and the weights and biases, which correspond to minimum prediction error for validation set were restored. The third set of data, the test set, was used for comparison of the performances of the trained networks.

When dividing the data into different sets randomly (as we did), it is useful to monitor not only validation but also the test set error during the training process. If the error in the test set reaches minimum at significantly different iteration number than validation set error, this may indicate the division of the data set is poor and should be redone.

The mean, minimal values for *RMSEP* for the test set applied on the trained neural networks as a function of number of hidden neurons are presented in Fig. 2. This figure shows that at the beginning the mean *RMSEP* for feed-forward networks (line) decreases as the number of hidden neurons increases and reaches minimum at value three hidden neurons ($RMSEP=0.0480 \text{ \AA}$) which indicates the network with best average performances. The mean *RMSEP* for cascade-forward networks is the smallest for the network with two hidden neurons ($RMSEP=0.0417 \text{ \AA}$). The prediction abili-

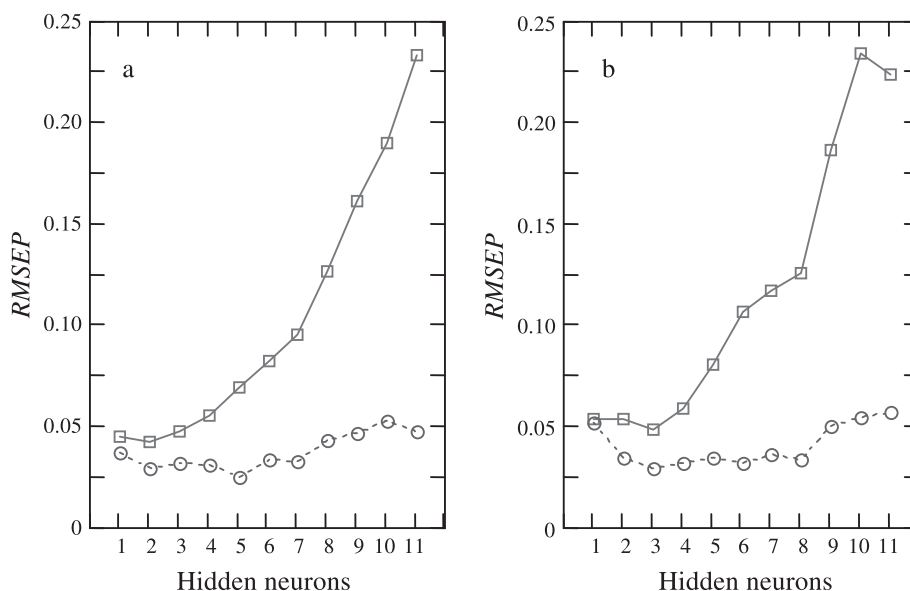


Fig. 2. Mean (—□—) and minimal (---○---) root mean square error for different ANN as a function of number of neurons in the hidden layer (a—cascade-forward and b—feed-forward networks).

ties of the both types of the ANNs were compared using F -test [43].

$$F(n_1, n_2) = RMSEP_1^2 / RMSEP_2^2 \quad (3)$$

In Eq. (3), n_1 and n_2 are the number of samples in the test set, $RMSEP_1^2$ is the square from the higher and $RMSEP_2^2$ is the square from lower root mean square error from the two compared. The calculated F -value (1.326) is lower than the critical one (2.014). The results show that at level of significance of 0.95 the differences in the performances of the mean $RMSEP$ in both network architectures differ only randomly. The feed-forward ANN with best performances has also three hidden neurons (0.0289 Å), but the cascade-forward ANN with minimal $RMSEP$ has five hidden neurons (0.0251 Å), probably due to chance effects

where the model fits local region of under fitting, which substantiates the claims of Laurence and Giles [44].

3.3. Comparison of the results

The agreement between the predicted (by all techniques) and experimental data is presented in Fig. 3 as well as the corresponding adjusted correlation coefficients. Comparison of the ANN and MLR models was done using their overall $RMSEP$. The presented $RMSEP$ values on Table 2 for both types of ANN are the one from the networks with best performances. In order to compare the performances of the different models the F -test was applied (Table 3). When comparing MLR with CF-ANN F -value (2.760) is higher than the critical one (2.014)

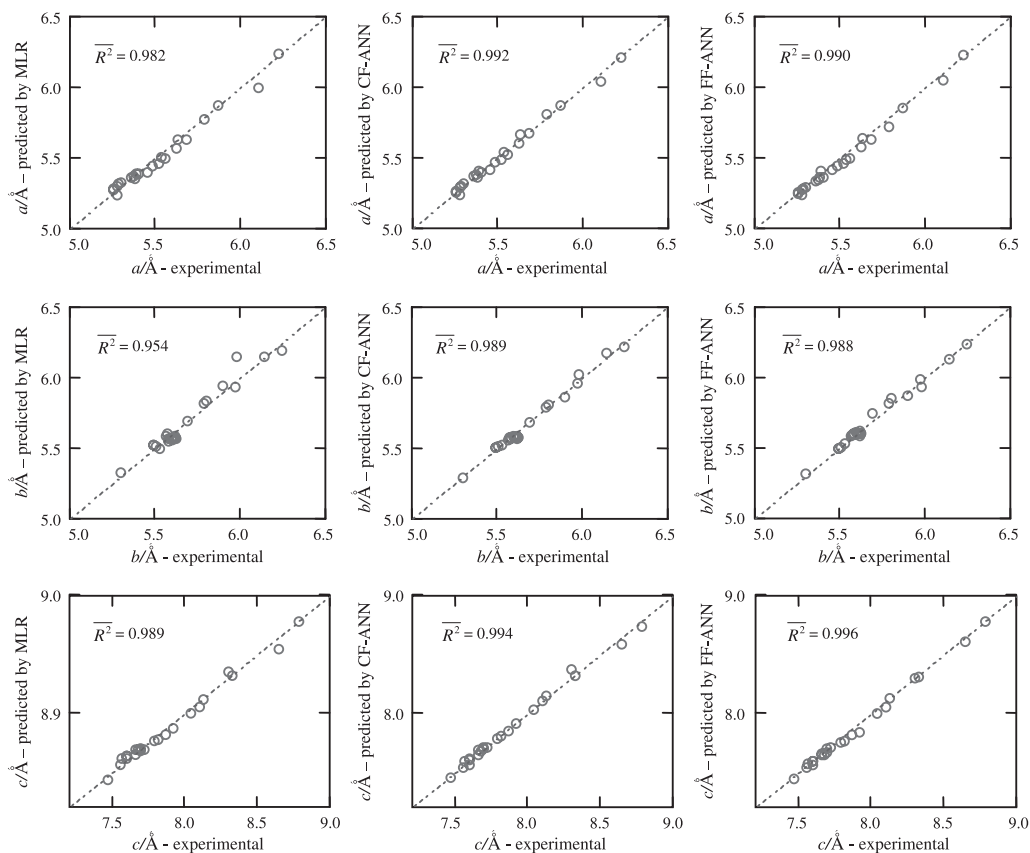


Fig. 3. Experimental versus predicted unit cell parameters with MLR, CF-ANN and FF-ANN.

Table 3

Comparison of different models using *F*-test (at level of significance 0.95)

Compared models	Calculated <i>F</i> -value	Calculated <i>F</i> -value
MLR/CF-ANN	2.760	2.014
MLR/FF-ANN	2.082	2.014
FF-ANN/CF-ANN	1.326	2.014

at level of significance of 0.95 the difference. When comparing MLR to FF-ANN, using *F*-test, the calculated *F*-value (2.082) compared to critical one shows statistically significant difference at level of significance of 0.95.

4. Conclusion

Feed-forward and cascade-forward artificial neural networks were used for prediction of unit cell parameters of orthorhombic perovskites as a function of the effective ionic radii of the constituents. Three-layered ANNs where the initial weights and biases were initialized using Nguyen–Widrow algorithm were optimized changing the number neurons in the hidden layer from 1 to 11, according to Levenberg–Marquardt algorithm for back-propagation of error. The feed-forward neural networks with three hidden neurons show the best average performances. The best average performances of the cascade-forward neural networks correspond to the architectures with two hidden neurons. No significant difference between average performances of the both types of the networks are noticed at level of significance of 0.95. Comparison of the results obtained by the best networks (of both types of ANNs) with the one obtained by MLR shows significant difference of the performances of the ANNs (at level of significance 0.95).

All three techniques show good results and can be used for predicting the unit cell parameters of new perovskites, as was successfully shown in our previous results for some other series of isomorphous compounds [3–6]. Here, we conclude that because of their capabilities to model appearing nonlinearities in the relationship between ionic radii and the unit cell parameters, artificial neural networks are capable of better prediction of the unit cell parameters compared to MLR.

References

- [1] F.C. Galasso, Structure, Properties and Preparation of Perovskite-type Compounds, Pergamon, 1969.
- [2] E.J. Baran, Catal. Today 8 (1973) 331 (and the references therein).
- [3] V. Petruševski, S. Aleksovska, Croat. Chem. Acta 67 (1994) 221.
- [4] S. Aleksovska, V. Petruševski, L.J. Pejov, Croat. Chem. Acta 70 (1997) 1009.
- [5] S. Aleksovska, S.C. Nyburg, L.J. Pejov, V.M. Petruševski, Acta Crystallogr. B54 (1998) 115.
- [6] S. Aleksovska, V.M. Petruševski, B. Šoptarjanov, Acta Crystallogr. B54 (1988) 564.
- [7] L. Hadjiiski, P. Geladi, P. Hopke, Chemometr. Intell. Lab. Syst. 49 (1999) 91.
- [8] A. Bos, M. Bos, W.E. van der Linden, Anal. Chim. Acta 256 (1992) 133.
- [9] J. Zupan, J. Gasteiger, Neural Networks in Chemistry and Drug Design, WCH, Weinheim, 1999.
- [10] R.D. Shannon, Acta Crystallogr. A32 (1976) 751.
- [11] J.M. Longo, Natl. Bur. Stand. (U.S.) Spec. Publ. 364 (1972) 219.
- [12] M. Marezio, J.D. Remeika, P.D. Dernier, Acta Crystallogr. B26 (1970) 2008.
- [13] J. Pickardt, Th. Schnedler, M. Kolm, Z. Anorg. Allg. Chem. 560 (1988) 153.
- [14] M. Fancher, P. Caro, Mater. Res. Bull. 10 (1975) 243.
- [15] S. Geller, Acta Crystallogr. 10 (1957) 243.
- [16] J.B. Clark, P.W. Richter, L. Du Toit, J. Solid State Chem. 23 (1978) 129.
- [17] G.V. Bazuev, G.P. Shveikin, Neorg. Mater. 11 (1975) 1333.
- [18] W. Sinclair, R.A. Eggleton, A.E. Ringwood, Z. Kristallogr. 149 (1979) 307.
- [19] M. Masao, Y. Toyooka, N. Tatsuo, Yogyo Kyokai Shi 85 (1977) 374.
- [20] R. Dieht, G. Brandt, Mater. Res. Bull. 10 (2) (1975) 85.
- [21] N.N. Sirota, A.P. Karavai, Vesti Akad. Nauk. BSSR, Ser. Fiz-Mat. Nauki 2 (1978) 74.
- [22] G.P. Shveikin, G.V. Bazuev, Zh. Neorg. Khim. 18 (2) (1973) 291.
- [23] N. Rosow, J.W. Lynn, Q. Lin, G. Cao, J.W. O'Reilly, P. Perambuco-Wise, J.E. Crow, Phys. Rev., B 45 (1992) 982.
- [24] G.G. Cristoph, A.C. Larson, P.G. Eller, J.D. Purson, J.D. Zahrt, R.A. Penneman, G.R. Rinehart, Acta Crystallogr. B44 (1988) 575.
- [25] R.H. Buttner, E.N. Maslen, Acta Crystallogr. B48 (1992) 639.
- [26] V.P. Dravid, C.M. Sung, M.R. Notis, C.E. Lyman, Acta Crystallogr. B45 (1989) 218.
- [27] S. Sasaki, C.T. Prewitt, J.D. Bass, W.A. Schulze, Acta Crystallogr. C43 (1987) 1668.
- [28] V.P. Redko, A.B. Shevchenko, L.M. Lopato, Neorg. Mater. 24 (1988) 2027.
- [29] C.W. Jones, P.D. Battle, P. Lightfoot, Acta Crystallogr. C45 (1989) 365.
- [30] M. Ahtee, A.W. Hewat, Acta Crystallogr. B32 (1976) 3243.

- [31] G.V. Bazuev, V.G. Zubkov, N.N. Iutin, G.P. Schveikin, *Zh. Neorg. Chim.* 21 (1976) 3235.
- [32] T. Peterlin-Neumaier, E. Steichele, *Spez. Ber. Kernforsch. Anl. Jul.* 316 (1985) 272.
- [33] Z.A. Zaitseva, A.L. Litvin, *Dopov. Akad. Nauk. Ukr. RSR, Ser. B: Geol. Khim. Biol. Nauki* 11 (1978) 994 (C.A. 90: 46925s).
- [34] S. Geller, A.E. Wood, *Acta Crystallogr.* 9 (1956) 563.
- [35] A.J. Jacobson, B.C. Tofield, B.E.F. Fender, *Proc. Rare Earth Res. Conf.* 10 (1973) 149.
- [36] A. Vegas, M. Vallet-Regí, J.M. Gonzales-Calbet, M.A. Alario-Franco, *Acta Crystallogr.* B42 (1986) 167.
- [37] E.A. Sololovleva, A.M. Garvish, I.V. Gluko, E.N. Zoz, *Neorg. Mat.* 10 (1974) 184.
- [38] H.L. Keller, K.H. Meier, H.K. Mueller-Busehbaum, *Z. Naturforsch., B, Anorg. Chem., Org. Chem.* 30B (1975) 277.
- [39] STATGRAPHICS PLUS, Ver. 3.0, Statistical Graphics Package, Educational Institution Edition, Statistical Graphics, 1994–1997.
- [40] Matlab 6.0, Mathworks, 1984–2000.
- [41] H. Demuth, M. Beale, *Neural Network Toolbox*, Mathworks, Natick, MA, 2000.
- [42] F. Despaigne, D.L. Massart, *Analyst* 123 (1998) 157R.
- [43] P. Bhandare, Y. Mendelson, R.A. Peura, G. Janatsch, J.D. Kruse-Jarres, R. Marbach, H.M. Heise, *Appl. Spectrosc.* 47 (1993) 1214.
- [44] S. Lawrence, C. Giles, in: S. Amari, C. Giles, M. Gori, V. Piuri (Eds.), *International Joint Conference on Neural Networks, Proceedings of the Conference, 24–27 July 2000, Como, Italy*. IEEE, vol. 114, 2000.